ADVANCED ENERGY MATERIALS

www.advenergymat.de

Tailoring Triple-Anion Perovskite Material for Indoor Light Harvesting with Restrained Halide Segregation and Record High Efficiency Beyond 36%

*Rui Cheng, Chih-Chun Chung, Hong Zhang, Fangzhou Liu, Wei-Ting Wang, Zhiwen Zhou, Sijia Wang, Aleksandra B. Djurišić, and Shien-Ping Feng**

Indoor photovoltaics are promising to enable self-powered electronic devices for the Internet of Things. Here, reported is a triple-anion $CH_3NH_3PbI_{2-x}BrCl_x$ perovskite film, of which the bandgap is specially designed for indoor light harvesting to achieve a record high efficiency of 36.2% with distinctive high open circuit voltage (V_{oc}) of 1.028 V under standard 1000 lux fluorescent light. The involvement of both bromide and chloride suppresses the trap-states and nonradiative recombination loss, exhibiting a remarkable ideality factor of 1.097. The introduction of chloride successfully restrains the halide segregation of iodide and bromide, stabilizing the triple-anion perovskite film. The devices show an excellent long-term performance, sustaining over 95% of original efficiency under continuous light soaking over 2000 h. These findings show the importance and potential of I/Br/Cl triple-anion perovskite with tailored bandgap and suppressed trap-states in stable and efficient indoor light recycling.

As the power required for the electronic device (e.g., sensors, actuators) continues to decrease, the use of indoor photovoltaic cells to power billions of wireless devices to collect the big data for a future Internet of Things (IoT) nodes is becoming possible, of which the self-powered characteristic can reduce the use of batteries and avoid battery replacement.[1–4] Organic photovoltaics (OPV), dye-sensitized solar cells (DSSC), and III-V solar cells (III-V SC) have been successfully demonstrated for converting indoor light into electricity. Especially, novel device structures and absorbers have pushed the efficiency of OPV, DSSC, and III-V SC up to 28.1%, 31.8%, and 21.0% under indoor light condition, respectively.[5–7] As a new member in the solar cell field, metal halide perovskite solar cells (PVSCs) should also be a promising candidate due to its high absorption coefficient, long carrier lifetime, low recombination rate, and outstanding power conversion efficiency (PCE).[8–11]

Indoor light, also called dim-light, ambient-light, or artificial light, has a power density with hundreds or thousands of times lower than 1 sun condition, which is usually defined as 1000 lux fluorescent or light-emitting diodes (LEDs) lights in the literatures as standard light source for indoor photovoltaic cells.[3,12,13] In such condition, the trap-control plays a key role in efficient indoor light harvesting. Different from numerous photo-generated electrons under 1 sun condition, the low incident power of indoor light could only generate a relatively small amount of electrons and therefore the trap-state density becomes critical due to a higher ratio of trapped-electron to photo-generated electrons. The major research work of PVSC has been conducted under 1 sun illumination, but studies focusing on indoor light harvesting are relatively few. Chen et al. modified the fabrication process to reduce the trap density at perovskite/[6,6]-phenyl-C_{61}-butyric acid methyl ester ($PC_{61}BM$) interface to realize an indoor PCE (i-PCE) of 27%.[12] Similarly, Dagar et al. reduced the trap-states of SnO_2/perovskite interface by introducing a MgO interlayer to achieve 26.9% i-PCE.[14] Furthermore, Li et al. employed 1-butyl-3-methylimidazolium tetrafluoroborate ($[BMIM]BF_4$) as the modification layer to pave the interface contact and passivate the surface trap-states of $PC_{61}BM$/Ag and realized an excellent 35.2% i-PCE.[15] Apart from the reduction of trap-states at interfaces, our previous work developed an air-knife-assisted recrystallization process with trap-healing capability, which successfully suppressed the trap-state density in the perovskite active layer and reached 27% i-PCE.[16]

Most of the abovementioned works have demonstrated high PCE over 18% under 1 sun condition but their i-PCE is

R. Cheng, Dr. C.-C. Chung, Dr. W.-T. Wang, Z. Zhou, S. Wang, Prof. S.-P. Feng
Department of Mechanical Engineering
The University of Hong Kong
Pokfulam Road, Hong Kong
E-mail: hpfeng@hku.hk

Dr. H. Zhang
Laboratory of Photonic and Interfaces
Ecole Polytechnique Fédérale de Lausanne (EPFL)
Lausanne 1015, Switzerland

Dr. F. Liu, Prof. A. B. Djurišić
Department of Physics
The University of Hong Kong
Pokfulam Road, Hong Kong

Prof. S.-P. Feng
Laboratory for Nanofluids and Thermal Engineering
HKU-Zhejiang Institute of Research and Innovation
Hangzhou 311305, China

The ORCID identification number(s) for the author(s) of this article can be found under https://doi.org/10.1002/aenm.201901980.

DOI: 10.1002/aenm.201901980

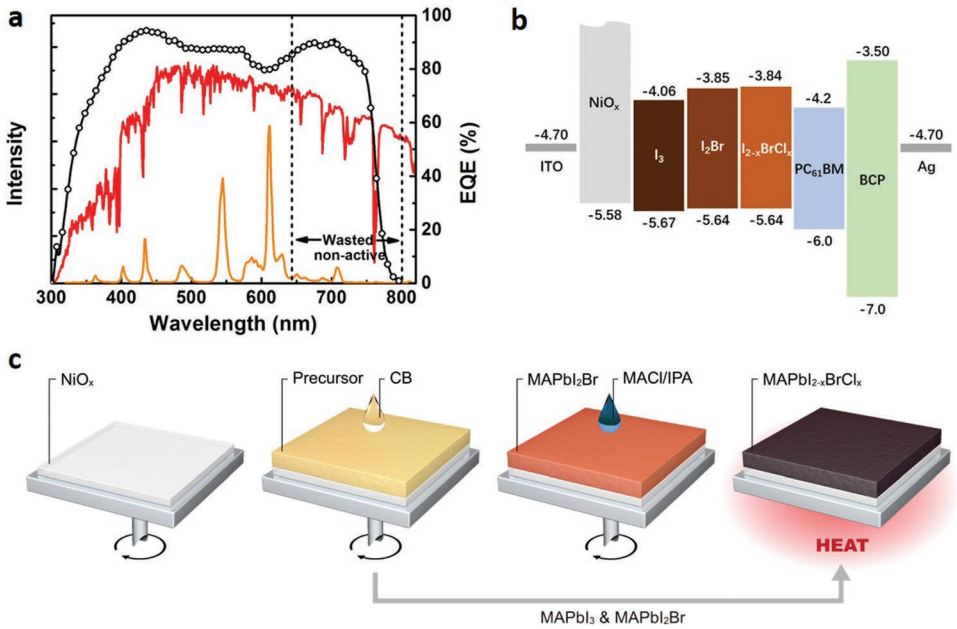

Figure 1. Compositional engineering of triple-anion perovskite material. a) Spectrum of solar light (red), 2700 K fluorescent light (orange), and IPCE curve (black) of a common $MAPbI_3$ perovskite device. The mismatched range (650–800 nm) between the fluorescent light spectrum and IPCE curve is nonactive and would not contribute to the photocurrent under indoor light, left a room to further enhance indoor PCE by enlarging the perovskite bandgap. b) Band alignment of the $MAPbI_3$, $MAPbI_2Br$, and $MAPbI_{2-x}BrCl_x$ devices. The energy level of all three perovskite materials well fit with the charge transport layers (NiO_x and $PC_{61}BM$) without charge extraction barriers. c) Schematic illustration of the fabrication process for the perovskite films. The $MAPbI_3$ and $MAPbI_2Br$ films were annealed right after one-step process, while an extra step of drop-casting MACl/IPA solution on top of the preformed $MAPbI_2Br$ films was needed to fabricate $MAPbI_{2-x}BrCl_x$ films.

usually less than 30%. It is worth noting that all these works are based on $CH_3NH_3PbI_3$ ($MAPbI_3$, $MA^+ = CH_3NH_3^+$) material with bandgap around 1.6 eV, of which the absorption edge is up to ≈780 nm; therefore, it is designed for solar illumination but may not be optimized for indoor light conditions. As shown in **Figure 1**a, the spectrum of fluorescent lamps is cut off at ≈640 nm. The mismatch between external quantum efficiency (EQE) curve and fluorescent light spectrum in a range of 640–800 nm is nonactive and would not contribute to the photocurrent of the device under indoor light. Hence, we believe that the PVSCs used for outdoor and indoor applications should be differentiated with the proper design to maximize their performances; there is a room to enlarge the bandgap by engineering the halide compositions specialized for indoor light harvesting;[17–20] by which, a designed perovskite material with tailored bandgap and suppressed trap states can attain a higher i-PCE with increased open circuit voltage (V_{oc}) and minimal short-circuit current (J_{sc}) loss.

Here, we report a stable $CH_3NH_3PbI_{2-x}BrCl_x$ triple-anion perovskite with a tailored bandgap of around 1.8 eV and ultralow trap-state density, achieving a record high i-PCE over 36% under 1000 lux fluorescent light. First, the bandgap is designed by adjusting the composition ratios of Br and Cl to well fit the indoor light spectrum; the involvement of both Br and Cl contribute to an enlarged bandgap and at the same time reduced trap-states of perovskite active layer, leading to the prolonged charge carrier lifetime, the suppressed nonradiative recombination, and the improved ideality factor. Second, the introduction of Cl restrained the halide segregation of I and Br during aging, significantly benefiting to the long-term device stability; additionally, the Cl-induced progressive crystallization not only enhanced the crystallinity of perovskite layer but also improved the NiO_x/perovskite interface to reduce the interfacial trap-states. All these factors contribute to the high i-PCE with V_{oc} of 1.028 V. To the best of our knowledge, this is the first study reported the strategy of synthesizing a I/Br/Cl triple-anion mixture perovskite for bandgap tuning and phase stabilizing. Our work paves a way in realizing a stable and high-efficiency indoor PVSCs to potentially fulfill a large network of self-powered devices for IoTs.

The typical inverted planar structure ITO (indium tin oxide)/NiO_x/perovskite/$PC_{61}BM$/bathocuproine(BCP)/Ag devices were used in this study. Low-temperature solution-combustion-based NiO_x was used as an efficient hole transport layer.[21] Three different kinds of perovskite materials: $MAPbI_3$, $MAPbI_2Br$, and $MAPbI_{2-x}BrCl_x$ were synthesized by one-step anti-solvent method. Figure 1b shows the band alignment of the perovskite cells, derived from the characterization results of ultraviolet photoelectron spectroscopy (UPS, Figure S1, Supporting Information) and UV-vis spectroscopy (Figure S2, Supporting Information). Figure 1c shows a schematic representation of the fabrication of perovskite layers. The perovskite mixed precursors were first dropped on NiO_x-coated ITO-glass substrates, followed by spin-coating and drop-casting of anti-solvents. After that, the $MAPbI_3$ and $MAPbI_2Br$ films were annealed immediately, while an extra step of drop-casting MACl/IPA solution on top of the preformed $MAPbI_2Br$ films was needed to fabricate $MAPbI_{2-x}BrCl_x$ films. The involvement of both bromide and chloride enlarged the bandgap from 1.61 eV ($MAPbI_3$) to 1.79 eV ($MAPbI_2Br$) and 1.80 eV ($MAPbI_{2-x}BrCl_x$). As observed

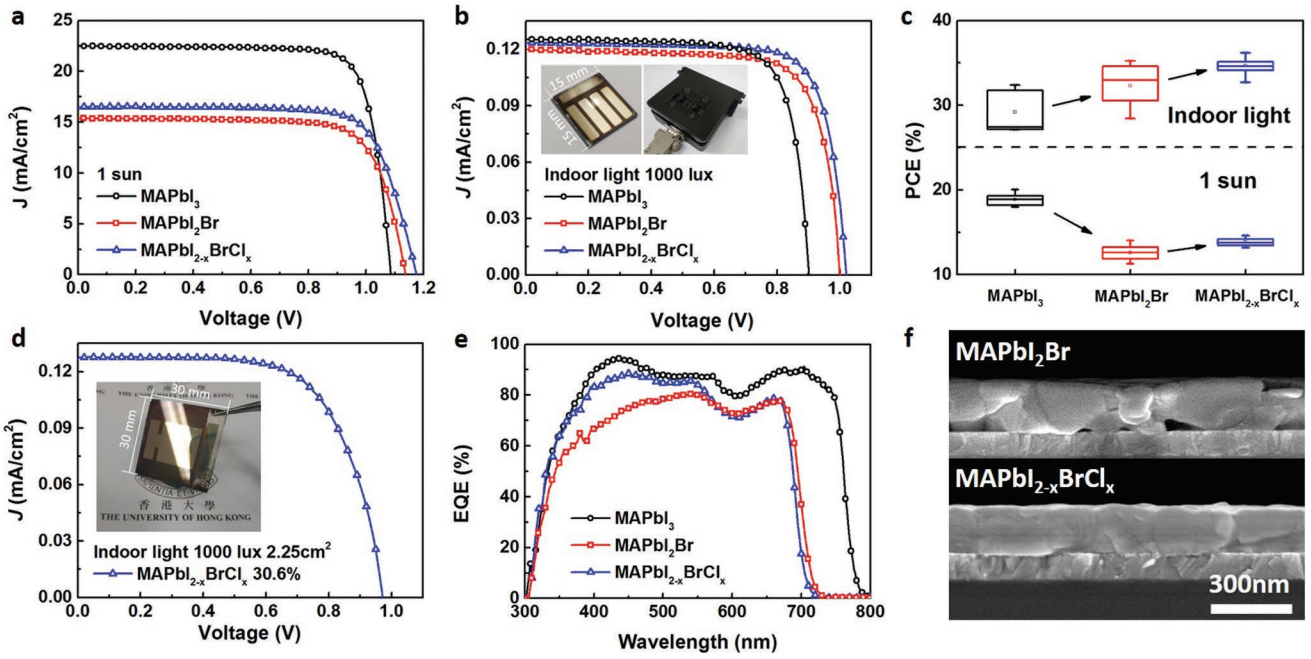

Figure 2. Tailored bandgap specialized for indoor light harvesting. a) *J–V* curves of $MAPbI_3$, $MAPbI_2Br$, and $MAPbI_{2-x}BrCl_x$ devices under 1 sun illumination. b) *J–V* curves of the three groups of devices under 1000 lux indoor light (2700 K fluorescent), evidencing the necessity of tuning bandgap in realizing record high i-PCE; inset shows the PVSC device (1.5×1.5 cm^2) and the test holder for 0.1 cm^2 active area. c) The statistics of PCE for the three groups of devices under 1 sun and indoor light conditions, respectively. d) *J–V* curve of the large area device (3×3 cm^2 with active area of 1.5×1.5 cm^2) under 1000 lux indoor light (2700 K fluorescent). e) IPCE of the three groups of devices. $MAPbI_2Br$ device has a relatively low EQE value, particularly the part of short wavelength in a range of 300–550 nm, attributing to the poor NiO_x/perovskite interface, which is facilely improved by MACl post-treatment. f) SEM cross-sectional views of $MAPbI_2Br$ and $MAPbI_{2-x}BrCl_x$ films.

in the band alignment, all three perovskite materials had similar valance band positions (−5.67, −5.64, −5.64 eV), correlating to that of NiO_x (−5.58 eV) for efficient hole extraction. However, the conduction band position moved to −3.85 and −3.84 eV due to the enlarged bandgap, which were 0.35 and 0.36 eV higher than the conduction band of $PC_{61}BM$, facilitating the electron extraction.

Based on our inference, the perovskite material with a high PCE under 1 sun condition might not be the best choice for indoor light harvesting because it exists unneglectable non-active absorption in the long-wavelength range. Instead, a designed perovskite layer with tailored bandgap has a potential to cut-off this range and boost-up V_{oc} to realize a higher i-PCE. Here, the device performances of $MAPbI_3$, $MAPbI_2Br$, and $MAPbI_{2-x}BrCl_x$ were measured under 1 sun illumination and 1000 lux 2700 K fluorescent light, as shown in **Figure 2**a,b, respectively.

The power density of the 2700 K warm white fluorescent light used in this work was calibrated by spectrum microscope, luminosity function, and lux meter (Figure S3 and Note S1, Supporting Information); the exact integrated power density under 1000 lux is 275.4 μW cm^{-2}, which is almost the same with the reported data.[5,15] The champion $MAPbI_3$ device has an excellent PCE of 20.0% under 1 sun illumination, which is relatively high among the reported MA-based PVSCs, indicating a high quality of our device. However, it only exhibits a i-PCE of 31.4%. In contrast, $MAPbI_2Br$ device shows a higher i-PCE of 33.0%, and $MAPbI_{2-x}BrCl_x$ device achieves a record high i-PCE of 36.2%, while these two devices can only reach PCE of 13.2% and 14.6% under 1 sun condition, respectively. Such contrary tendency is resulted from the spectrum-dependent performance of the devices. The relatively wide absorption of $MAPbI_3$ better fits the solar radiation spectrum and allows a high J_{sc} to realize a high PCE; the tailored bandgap of $MAPbI_{2-x}BrCl_x$ better fits the indoor light spectrum and obtains a large V_{oc} to achieve a high i-PCE. It is noted that the absorption range of both devices completely covered the indoor light spectrum, resulting in comparable photocurrents under indoor condition. In detail, the $MAPbI_3$ device shows V_{oc} of 0.901 V under indoor light which is lower than 0.999 V of $MAPbI_2Br$ device and 1.028 V of $MAPbI_{2-x}BrCl_x$ device; all three groups of devices show similar J_{sc} (125.2, 120.2, 123.7 μA cm^{-2}), evidencing that the improvement of V_{oc} plays a major role to enhance the i-PCE of PVSCs. Hence, through bandgap engineering, our triple-anion perovskite material with tailored bandgap specialized for indoor light demonstrated a higher V_{oc} and comparable J_{sc}, resulting a superior performance. Figure 2c shows the statistics of PCE for the three groups of devices under 1 sun and indoor light conditions, respectively, demonstrating a substantial improvement of i-PCE based on our strategy. The indoor performance was found to be more scattered as compared with 1 sun performance. During the perovskite fabrication, it is inevitable to have a variation of the trap-state density from one sample to another. Unlike 1 sun condition, the trap-state density plays a decisive role in PCE under indoor light condition so that the varied trap-state densities among samples cause a more scattered PCE distribution. Figure 2d shows the *J–V* characteristic of the large area device under indoor light. The 3×3 cm^2 device

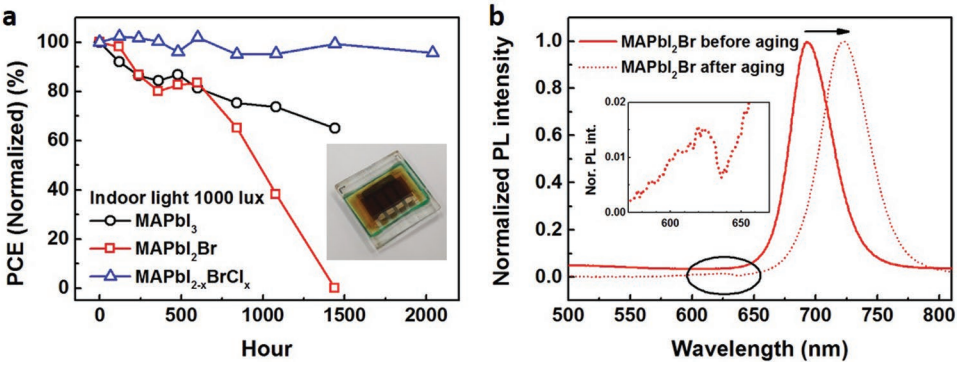

Figure 3. Stable triple-anion perovskite without ion segregation. a) Evolution of i-PCE as compared with the initial parameters for the encapsulated devices under continuous light soaking. The $MAPbI_3$ device shows a typical moderate degradation curve; the $MAPbI_2Br$ device severely degraded due to the segregation of I/Br; the $MAPbI_{2-x}BrCl_x$ device sustained over 95% of original i-PCE, suggesting that the involvement of Cl ion is crucial to inhibit the segregation of I/Br; inset shows the encapsulated PVSC device. b) The PL shifting of the $MAPbI_2Br$ device before and after aging for 60 days, evidencing the photo-induced I/Br segregation.

with 2.25 cm^2 active area also demonstrates over 30% i-PCE with output power of 189.8 μW. Figure 2e is the EQE curve from the incident photon-to-electron conversion efficiency (IPCE) characterization for the three groups of devices. As seen, the absorption edge of perovskite device was blue-shifted from 778 nm of MAPbI3 to 714 nm of $MAPbI_2Br$ and 705 nm of $MAPbI_{2-x}BrCl_x$, indicating that the introduction of both Br and Cl contributes to the increased bandgap. The photocurrent was integrated based on IPCE (Figure S4, Supporting Information). When counting up to 800 nm, $MAPbI_3$ device shows obviously higher integrated current than $MAPbI_2Br$ and $MAPbI_{2-x}BrCl_x$; on the other hand, when integrating from 300 to 640 nm, three groups of devices have comparable values. The result is consistent with the *J–V* curves shown in Figure 2a,b with distinguishable J_{sc} under 1 sun and similar J_{sc} under indoor light, respectively. $MAPbI_2Br$ device has a relatively low EQE value, particularly the part of short wavelength in a range of 300–550 nm. In Figure 2f, scanning electron microscope (SEM) characterization found numbers of holes occurred at the $NiO_x/MAPbI_2Br$ interface, which may come from the instantaneous crystallization of Br-contained perovskite during one-step fabrication and cause inefficient charge extraction from perovskite layer to bottom layer (Figure S5, Note S2, Supporting Information). Although our strategy of bandgap engineering could be simply realized by adjusting I/Br ratio to form $MAPbI_{3-x}Br_x$ with tailored bandgap, the poor interfacial contact limits the device performance. By introducing a MACl post-treatment on the preformed $MAPbI_2Br$ film right after one-step fabrication, MACl would quickly react with the preformed film to form intermediate phase of $MAPbI_aBr_bCl_{3-a-b}$.[16,22–24] During annealing, the intermediate-phase perovskite would progressively recrystallize to form highly crystalline perovskite. The relatively slow volume expansion can fill up the holes left by *N,N*-dimethylformamide (DMF) evaporation to construct an intact $NiO_x/MAPbI_{2-x}BrCl_x$ interface (Figure 2f), resulting in the enhanced EQE value from 300 to 550 nm. SEM energy-dispersive X-ray spectroscopy (EDX) mapping was used to examine the $MAPbI_{2-x}BrCl_x$ perovskite film (Figure S6, Supporting Information), providing evidence that all the involved ions (e.g., Pb, I, Br, Cl) were uniformly distributed in the film. Although Cl was introduced by post-treatment from the upper surface, it was well diffused through the bulk film after recrystallization. The optimization of MACl post-treatment was done by experimenting the different concentrations of MACl/IPA solution (Figure S7 and Note S3, Supporting Information). Moreover, based on the photoluminescence (PL) characterizations (Figure S8, Supporting Information), the individual $MAPbI_2Br$ and $MAPbI_{2-x}BrCl_x$ films show comparable PL intensity; on the other hand, $NiO_x/MAPbI_{2-x}BrCl_x$ has a lower PL intensity as compared with $NiO_x/MAPbI_2Br$, suggesting a better hole extraction performance benefiting from the improved NiO_x/perovskite interface.

Other than a high efficiency, the device long-term stability is essential to real applications. It has been reported that photo-induced and current-induced halide segregation usually happens in mix-halide perovskite systems, which is one of the major reasons for performance degradation;[25–28] such issue is particularly important in our triple-anion material. To investigate the i-PCE degradation, the $MAPbI_3$, $MAPbI_2Br$, and $MAPbI_{2-x}BrCl_x$ devices were well encapsulated to avoid external influences except halide segregation, and were then kept under continuous light soaking (1000 lux fluorescent light).[29] As shown in **Figure 3**a, the $MAPbI_3$ devices show a typical moderate degradation curve and remained 65.0% of original i-PCE after aging for 60 days. The $MAPbI_2Br$ devices were severely degraded to 38.3% of original i-PCE after 45 days and were collapsed after 60 days, attributing to the halide segregation.

Figure 3b shows the PL of the $MAPbI_2Br$ device before and after aging for 60 days. The device was immediately measured after taking apart from the encapsulation to avoid any other influences. The major PL peak was shifted from 693 to 723 nm after aging, while an additional small peak was occurred at 630 nm, indicating that the photo-induced I/Br segregation causes the formation of I-rich domains and Br-rich domains. The low-lying I-rich state would serve as recombination center to severely degrade the device performance, as consistent with the reported observations.[26] As observed, the $MAPbI_2Br$ device followed $MAPbI_3$ device to show a typical gentle degradation in the first 500 h according to the decomposition-dominated PCE degradation. After 500 h, the $MAPbI_3$ device

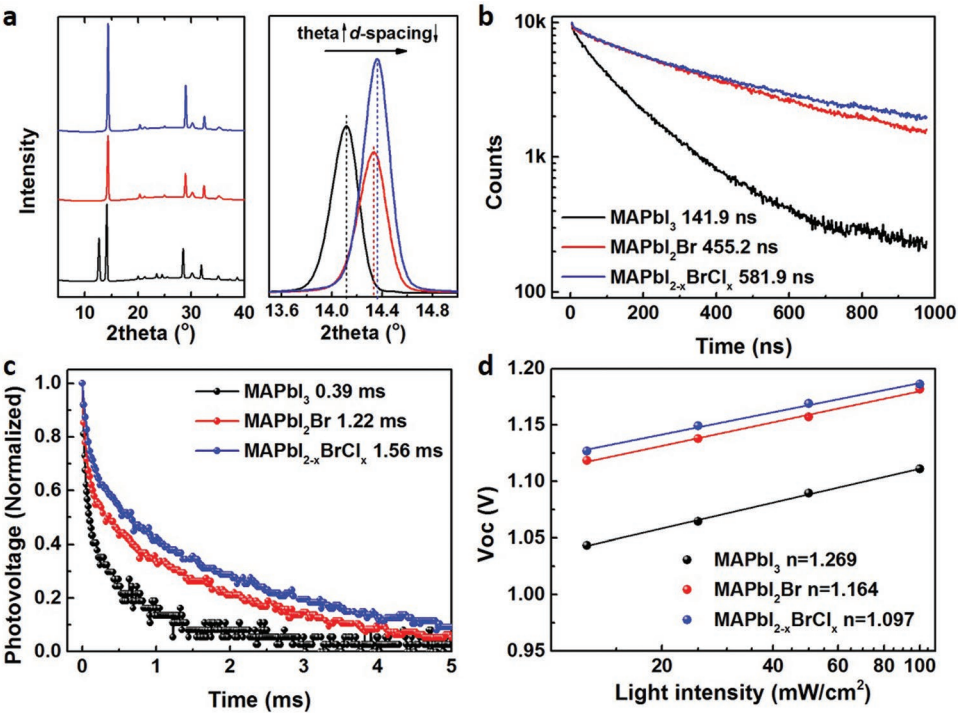

Figure 4. Characteristics of charge dynamics and recombination. a) XRD patterns of the devices, indicating the involvement of Br and Cl in the films and the enhancement of crystallinity by MACl post-treatment. b) TRPL decay of perovskite films, implying a considerable suppression of nonradiative recombination through Br and Cl involvement. c) Transient photovoltage decay under open circuit condition, the prolonged charge carrier lifetime corroborates the reduction of trap-states and recombination. d) V_{oc} as a function of light intensity for the calculation of ideality factor, our designed triple-anion device demonstrates the excellent ideality factor of 1.097.

kept its trend but the $MAPbI_2Br$ device severely degraded to 0, which should mainly come from the light-induced ion segregation. Impressively, $MAPbI_{2-x}BrCl_x$ devices sustained over 95% of original i-PCE after aging for 85 days without PL peak shifting (Figure S9, Supporting Information), suggesting that the involvement of Cl ion is crucial to inhibit the segregation of I and Br. Since Cl has a relatively small ionic radius (1.81 Å) compared with I (2.20 Å) and Br (1.96 Å), the involvement of Cl would induce a shrinkage of crystal lattice (Figure S10, Supporting Information). The shrinkage not only retarded the ion migration of I and Br, but also contributes to the enhancement of Pb-I and Pb-Br binding energy,[30] resulting in the restrained segregation and the improved stability. A similar phenomenon was observed by Saliba et al. in Cs/FA/MA triple-cation perovskite with phase stabilizing (α-phase) effect benefited from the difference of ionic radius among Cs, FA, and MA.[31] To the best of our knowledge, this is the first time to report a long-term stable and high-efficiency perovskite using I/Br/Cl triple-anion mixture system.

Trap-control also plays a key role in efficient indoor light harvesting. Different from numerous photo-generated electrons under 1 sun condition, the low incident power of indoor light could only generate a relatively small amount of electrons and therefore the trap-state density becomes critical due to a higher ratio of trapped-electron to photo-generated electrons. **Figure 4**a shows X-ray diffraction (XRD) data for $MAPbI_3$, $MAPbI_2Br$, and $MAPbI_{2-x}BrCl_x$ films. All three films exhibited a typical perovskite (110) peak at around 14°, which shifted from 14.12° ($MAPbI_3$) to 14.33° ($MAPbI_2Br$) and 14.36° ($MAPbI_{2-x}BrCl_x$), respectively. No $MAPbBr_3$ or $MAPbCl_3$ peaks were observed. According to Bragg's law

$$2d \sin\theta = n\lambda \quad (1)$$

the increased θ value corresponds to the decreased d-spacing, correlating to the involvement of small Br and Cl ions, respectively. Besides, the (110) peak intensity of $MAPbI_2Br$ film was almost doubled after the MACl post-treatment, demonstrating an enhanced crystallinity via Cl-induced progressive crystallization and contributes to a lower trap-states.

Figure 4b is the measurement of time-resolved PL (TRPL) to study the carrier recombination in the perovskite layers; the perovskite layers were directly deposited on bare quartz glass substrates without charge transport layers. The TRPL data were fitted by bi-exponential function (Table S1, Supporting Information), where τ_1 represents the carrier diffusion lifetime (fast decay) and τ_2 represents the radiative recombination lifetime of free electrons and holes (slow decay). τ_1 and τ_2 are the existing two major paths of recombination. τ_1 is prolonged with the involvement of Br and Cl, correlating to the prolonged carrier diffusion length and lower trap-states; the increased τ_2 indicates the improved crystal quality and reduced nonradiative recombination rate. The prolonged τ_{ave} represents the suppressed nonradiative recombination channels in the perovskite films, which is consistent with the enhanced PCE. The average carrier lifetime of $MAPbI_3$ is 141.9 ns; it increases to 455.2 ns when introducing

Br and raises up to 581.9 ns by further MACl post-treatment, implying a considerable suppression of nonradiative recombination for our designed perovskite material. The trap-healing effect of Cl was further investigated by calculating the trap-state density of $MAPbI_2Br$ and $MAPbI_{2-x}BrCl_x$ films through the space-charge-limited-current (SCLC) method using the electron-only device configuration of ITO/SnO_2/perovskite/$PC_{61}BM$/BCP/Ag (Figure S11, Supporting Information).[32] After involving Cl into $MAPbI_2Br$ film, the trap-state density was reduced from 1.04×10^{16} to 6.0×10^{15} cm^{-3}. The charge carrier recombination lifetime of the perovskite device was measured by transient photovoltage decay under open circuit condition, as shown in Figure 4c. As seen, the involvement of Br and Br/Cl significantly prolonged the charge recombination lifetime from 0.39 to 1.22 and 1.56 ms respectively, which corroborates the reduction of trap-states and recombination, as consistent with TRPL results. In Figure 4d, we investigated the relationship between V_{oc} and light intensity to calculate the ideality factor ($1 < n < 2$) based on the equation

$$n = \frac{q}{kT}\frac{dV_{oc}}{d\ln(\phi)} \quad (2)$$

providing a direct evidence to identify the dominant recombination mechanism of the devices. When n approaches to 1, the negligible recombination mainly comes from free electrons and holes; when n closes to 2, trap-assisted Shockley–Read–Hall (SRH) recombination is dominant.[31] Through linear fitting of $V_{oc}/\ln(\phi)$, the ideality factor n can be calculated as 1.269, 1.164, and 1.097 for $MAPbI_3$, $MAPbI_2Br$, and $MAPbI_{2-x}BrCl_x$, respectively. The gradual decrease of ideality factor approaching to 1 reveals that the involvement of both Br and Cl contributes to the reduced trap-assisted SRH recombination. Other than recombination, such ideality factor with the value close to 1 also represents the low rate of V_{oc} loss against light intensity, exhibiting a high V_{oc} under the dim indoor light. All the above-mentioned characterizations consistently demonstrated the high quality and low defect level of our designed perovskite films. Therefore, the design concept of this work not only strategically tuned the perovskite bandgap for adapting the indoor light sources, but also successfully suppressed the trap-states of perovskite devices. All these factors together contribute to achieve our stable and high-efficiency indoor PVSCs.

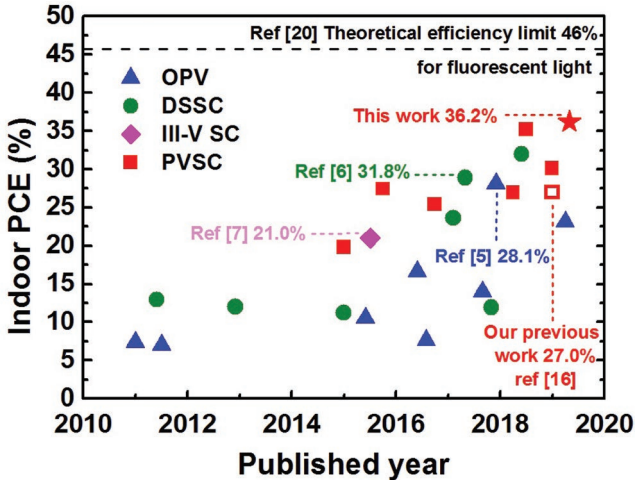

Figure 5. Summarized indoor PCE of representative works of OPV, DSSC, III-V SC, and PVSC.

Figure 5 and **Table 1** summarize the reported indoor photovoltaic cells, including the representative works of OPV, DSSC, III-V SC, and PVSC.[5,6,12,14–16,33–45] The more detailed information for indoor PVSCs is summarized in Table S2, Supporting Information. We have verified all the works listed in the table that most of them show comparable high EQE values; we therefore believe that the different photocurrent values possibly come from the use of diverse light sources with different power density and spectrum. Among all these works, our device exhibits a distinctive high V_{oc} of 1.028 V, which is about 9.4–30% higher than all the other reported works. Such high V_{oc} realizes the record high i-PCE of 36.2%, revealing the efficacy and necessity of tuning bandgap for efficient indoor light harvesting.

In summary, we have developed a stable $MAPbI_{2-x}BrCl_x$ triple-anion perovskite with a tailored bandgap and ultra-low trap-state density specialized for indoor light harvesting. The involvement of both Br and Cl enlarged the bandgap to better fit the indoor light spectrum, demonstrating a distinctive high V_{oc} of 1.028 V with negligible photocurrent loss; it also suppressed

Table 1. Reported representative indoor photovoltaic cells (OPV, DSSC, III-V SC, and PVSC).

Indoor PV cells	Light source	Color temperature [K]	Light intensity [lux]	Reported power density [μW cm^{-2}]	J_{sc} [μA cm^{-2}]	V_{oc} [V]	FF [%]	PCE [%]	Ref.
OPV	Osram L18W/827	2700	1000	278.7	133.1	0.79	75.2	28.1	[5]
DSSC	Osram Warm White 930	2700	1000	318.2	149.3	0.878	77.3	31.8	[6]
III-V SC	Osram Warm White 827	2700	1000	354.0	99.0	0.94	80.0	21.0	[7]
PVSC	Philip T5 6500K	6500	1000	310.0	137.5	0.85	77	27.4	[12]
	Osram Parathom Classic P25 LED	6500	400	154.6	64.5	0.895	72.0	26.9	[14]
	Osram L18W/827	2700	1000	278.7	150.1	0.87	75.2	35.2	[15]
	Philip T5 6500K	6500	1000	310.0	129.5	0.858	75.3	27.0	[16]
	Philip T5 6500K	6500	1000	310.0	139	0.91	75	30.1	[32]
	Philip T2 15W E27	2700	1000	275.4	126.2	1.028	76.8	36.2	This work

the trap-states and nonradiative recombination, contributing to the remarkable ideality factor of 1.097. The introduction of Cl effectively stabilized the perovskite film by restraining the ion segregation of I and Br. The device exhibits an excellent long-term stability with negligible i-PCE degradation under continuous light soaking over 2000 h. Based on this designed perovskite material, we realized a record high efficiency of 36.2% under 1000 lux fluorescent light, outperforming all the reported indoor photovoltaic cells. Our work leads to a new insight on tailoring triple-anion perovskite materials for stable and efficient indoor light harvesting, which paves a way to future large networks of connected self-powered devices for IoTs ecosystem.

Experimental Section

Materials: CH_3NH_3I, CH_3NH_3Br were purchased from Greatcell Solar Materials. PbI_2 (99.99%) was purchased from TCI. $PbCl_2$ (99.99%), BCP, 96%, DMF (anhydrous, 99.8%), chlorobenzene (CB, anhydrous, 99.8%), 1,2-dichlorobenzene (DCB, anhydrous, 99%), and isopropanol (IPA, anhydrous, 99.5%) were purchased from Sigma Aldrich. $PC_{61}BM$ (99.5%) was purchased from NANO-C. All the chemicals and materials were purchased and used as received.

Device Fabrication: ITO-glass substrate (15 mm × 15 mm) was first patterned and cleaned in turn by detergent, deionized water, and IPA for 20 min each, followed by ozone-plasma treatment for 5 min. The combustion-NiO_x precursor solution was prepared following the reported method,[21] and spin-coated on the substrate at 3000 rpm for 45 s and annealed at 250 °C for 45 min in air. After cooling down to room temperature, the NiO_x films were transferred to N_2-filled glove box for the following device fabrication process without any other treatment. The perovskite solutions were prepared by dissolving 500 mg PbI_2, 30 mg $PbCl_2$, and 190 mg MAI in 1 mL DMF for $MAPbI_3$ films; or 575 mg PbI_2 and 134 mg MABr in 1 mL DMF for $MAPbI_2Br$ and $MAPbI_{2-x}BrCl_x$ films. To deposit the perovskite film, the precursor solution was dropped on the NiO_x film and then spin-coated at 5000 rpm for 25 s. 180 µL CB was quickly dropped onto the substrate at the 6th s. For $MAPbI_{2-x}BrCl_x$ films, an extra step of MACl post-treatment was realized by dropping 0.066 M MACl/IPA onto the substrate at the 15th s. After that, the samples were annealed at 100 °C for 15 min. Subsequently, 20 mg mL^{-1} $PC_{61}BM$/DCB solution was spin-coated on top of perovskite at 1500 rpm for 60 s and annealed at 50 °C for 5 min. After cooling down to room temperature, 0.5 mg mL^{-1} BCP/ethanol was spin-coated at 4000 rpm for 20 s. Finally, 100 nm Ag electrode was deposited on top by thermal evaporation.

Measurement and Characterization: The EQE spectra were obtained using EQE measurement system (QE-R, Enli Technology), calibrated by standard single-crystal Si photovoltaic cell. The valance band position of the films was confirmed by UPS (ESCALAB Xi$^+$, Thermo Fisher) using a He discharged lamp (He I 21.22 eV). The perovskite bandgap was calculated using Tauc equation based on perovskite film absorption curve measured by UV-vis spectroscopy (Lambda 35, Perkin Elmer). The *J–V* characteristics of PVSCs were measured with Keithley 2400 sourcemeter under AM 1.5G solar illumination at an intensity of 100 mW cm^{-2} (PECL01 solar simulator, Peccell) and device active area of 0.1 cm^2. For indoor light conditions, Philip T2 15W E27 fluorescent lamp (2700 K warm white) was applied as light source, and the light intensity was calibrated to 1000 lux by lux meter (LX-105, YSC). Spectrum of the indoor light source was collected using a fiberoptic spectrometer (PDA-512USB, Control Development Inc.). The indoor light power density at 1000 lux was obtained based on light spectrum and luminosity function $\Phi = 683 \int \nu(\lambda) e(\lambda) d\lambda$ (Note S1, Supporting Information). SEM images and EDX mapping were obtained using scanning electron microscopy (S4800 FEG, Hitachi). The XRD measurement was carried out by X-ray diffractometer (Smartlab 9kw, Rigaku, Cu target λ = 1.5406 Å). The TRPL data were obtained by a spectrofluorometer (FLS 980, Edinburgh Instruments) with the exciton source of 485 nm laser, using perovskite film deposited directly on bare quartz substrate. For transient photovoltage decay, the complete perovskite device was under a double-frequency Nd:YAG pulse laser (530 nm); the signal was captured by a digital oscilloscope (HP54810A). The TRPL decay curves and transient photovoltage decay curves were fitted by bi-exponential function

$$I(t) = A_1 \exp\left(-\frac{t}{\tau_1}\right) + A_2 \exp\left(-\frac{t}{\tau_2}\right) \quad (3)$$

Room temperature PL measurements were performed with a HeCd (325 nm) laser as the excitation source, and the spectra were collected using a fiberoptic spectrometer (PDA-512USB, Control Development Inc.). The trap-state density was examined by the SCLC method using the electron-only device configuration of ITO/SnO_2/Perovskite/P_{61}CBM/BCP/Ag, using electrochemical workstation (CHI660, Shanghai Chenhua, current sensitivity 10^{-9} A).

Supporting Information

Supporting Information is available from the Wiley Online Library or from the author.

Acknowledgements

This work was supported by the General Research Fund of the Research Grants Council of Hong Kong Special Administrative Region, China under Award Number 17204516 and 17206518, and Environment and Conservation Fund (ECF 49/2017). This work was also supported by the Seed Fund for Strategic Interdisciplinary Research Scheme at the University of Hong Kong and HKU-Zhejiang Institute of Research and Innovation (HKU-ZIRI). The authors also thank Prof. Jun Zhang (Inner Mongolia University), Dr. Ji Tae Kim (the University of Hong Kong), and Dr. Sai Wing Tsang (City University of Hong Kong) for the support and assistance.

Conflict of Interest

The authors declare no conflict of interest.

Keywords

halide segregation, indoor light harvesting, perovskite solar cells, tailored bandgap, triple anion

Received: June 19, 2019
Revised: August 7, 2019
Published online: August 27, 2019

[1] Z. L. Wang, W. Wu, *Angew. Chem., Int. Ed.* **2012**, *51*, 11700.
[2] Z. L. Wang, *Adv. Mater.* **2012**, *24*, 280.
[3] X. Yue, M. Kauer, M. Bellanger, O. Beard, M. Brownlow, D. Gibson, C. Clark, C. MacGregor, S. Song, *IEEE Internet Things J.* **2017**, *4*, 2092.
[4] I. Mathews, S. N. Kantareddy, T. Buonassisi, I. M. Peters, *Joule* **2019**, *3*, 1415.
[5] H. K. H. Lee, J. Wu, J. Barbé, S. M. Jain, S. Wood, E. M. Speller, Z. Li, F. A. Castro, J. R. Durrant, W. C. Tsoi, *J. Mater. Chem. A* **2018**, *6*, 5618.
[6] Y. M. Cao, Y. H. Liu, S. M. Zakeeruddin, A. Hagfeldt, M. Gratzel, *Joule* **2018**, *2*, 1108.

[7] M. Freitag, J. Teuscher, Y. Saygili, X. Y. Zhang, F. Giordano, P. Liska, J. L. Hua, S. M. Zakeeruddin, J. E. Moser, M. Grätzel, A. Hagfeldt, *Nat. Photonics* **2017**, *11*, 372.
[8] Q. Q. Lin, A. Armin, R. C. R. Nagiri, P. L. Burn, P. Meredith, *Nat. Photonics* **2015**, *9*, 106.
[9] D. Shi, V. Adinolfi, R. Comin, M. Yuan, E. Alarousu, A. Buin, Y. Chen, S. Hoogland, A. Rothenberger, K. Katsiev, Y. Losovyj, X. Zhang, P. A. Dowben, O. F. Mohammed, E. H. Sargent, O. M. Bakr, *Science* **2015**, *347*, 519.
[10] G. Xing, N. Mathews, S. S. Lim, N. Yantara, X. Liu, D. Sabba, M. Gratzel, S. Mhaisalkar, T. C. Sum, *Nat. Mater.* **2014**, *13*, 476.
[11] Q. Jiang, Y. Zhao, X. Zhang, X. Yang, Y. Chen, Z. Chu, Q. Ye, X. Li, Z. Yin, J. You, *Nat. Photonics* **2019**, *13*, 460.
[12] C. Y. Chen, J. H. Chang, K. M. Chiang, H. L. Lin, S. Y. Hsiao, H. W. Lin, *Adv. Funct. Mater.* **2015**, *25*, 7064.
[13] F. De Rossi, T. Pontecorvo, T. M. Brown, *Appl. Energy* **2015**, *156*, 413.
[14] J. Dagar, S. Castro-Hermosa, G. Lucarelli, F. Cacialli, T. M. Brown, *Nano Energy* **2018**, *49*, 290.
[15] M. Li, C. Zhao, Z. K. Wang, C. C. Zhang, H. K. H. Lee, A. Pockett, J. Barbe, W. C. Tsoi, Y. G. Yang, M. J. Carnie, X. Y. Gao, W. X. Yang, J. R. Durrant, L. S. Liao, S. M. Jain, *Adv. Energy Mater.* **2018**, *8*, 1801509.
[16] R. Cheng, C. C. Chung, H. Zhang, Z. Zhou, P. Zhai, Y. T. Huang, H. Lee, S. P. Feng, *Small* **2019**, *15*, 1804465.
[17] I. E. Castelli, J. M. Garcia-Lastra, K. S. Thygesen, K. W. Jacobsen, *APL Mater.* **2014**, *2*, 081514.
[18] Q. Chen, N. De Marco, Y. M. Yang, T. B. Song, C. C. Chen, H. Zhao, Z. Hong, H. Zhou, Y. Yang, *Nano Today* **2015**, *10*, 355.
[19] L. Gil-Escrig, A. Miquel-Sempere, M. Sessolo, H. J. Bolink, *J. Phys. Chem. Lett.* **2015**, *6*, 3743.
[20] M. Freunek, M. Freunek, L. M. Reindl, *IEEE J. Photovoltaics* **2012**, *3*, 59.
[21] Z. Liu, J. Chang, Z. Lin, L. Zhou, Z. Yang, D. Chen, C. Zhang, S. Liu, Y. Hao, *Adv. Energy Mater.* **2018**, *8*, 1703432.
[22] J. Chae, Q. Dong, J. Huang, A. Centrone, *Nano Lett.* **2015**, *15*, 8114.
[23] Y. Xu, L. Zhu, J. Shi, S. Lv, X. Xu, J. Xiao, J. Dong, H. Wu, Y. Luo, D. Li, Q. Meng, *ACS Appl. Mater. Interfaces* **2015**, *7*, 2242.
[24] Q. Dong, Y. Yuan, Y. Shao, Y. Fang, Q. Wang, J. Huang, *Energy Environ. Sci.* **2015**, *8*, 2464.
[25] D. J. Slotcavage, H. I. Karunadasa, M. D. McGehee, *ACS Energy Lett.* **2016**, *1*, 1199.
[26] S. J. Yoon, S. Draguta, J. S. Manser, O. Sharia, W. F. Schneider, M. Kuno, P. V. Kamat, *ACS Energy Lett.* **2016**, *1*, 290.
[27] A. J. Barker, A. Sadhanala, F. Deschler, M. Gandini, S. P. Senanayak, P. M. Pearce, E. Mosconi, A. J. Pearson, Y. Wu, A. R. S. Kandada, T. Leijtens, F. De Angelis, S. E. Dutton, A. Petrozza, R. H. Friend, *ACS Energy Lett.* **2017**, *2*, 1416.
[28] M. C. Brennan, S. Draguta, P. V. Kamat, M. Kuno, *ACS Energy Lett.* **2018**, *3*, 204.
[29] Q. Dong, F. Liu, M. K. Wong, H. W. Tam, A. B. Djurišić, A. Ng, C. Surya, W. K. Chan, A. M. C. Ng, *ChemSusChem* **2016**, *9*, 2597.
[30] L. Fu, Y. Zhang, B. Chang, B. Li, S. Zhou, L. Zhang, L. Yin, *J. Mater. Chem. A* **2018**, *6*, 13263.
[31] M. Saliba, T. Matsui, J. Y. Seo, K. Domanski, J. P. Correa-Baena, M. K. Nazeeruddin, S. M. Zakeeruddin, W. Tress, A. Abate, A. Hagfeldt, M. Gratzel, *Energy Environ. Sci.* **2016**, *9*, 1989.
[32] H. Zhang, X. G. Ren, X. W. Chen, J. Mao, J. Q. Cheng, Y. Zhao, Y. H. Liu, J. Milic, W. J. Yin, M. Gratzel, W. C. H. Choy, *Energy Environ. Sci.* **2018**, *11*, 2253.
[33] C. Y. Chen, W. H. Lee, S. Y. Hsiao, W. L. Tsai, L. Yang, H. L. Lin, H. J. Chou, H. W. Lin, *J. Mater. Chem. A* **2019**, *7*, 3612.
[34] S. Mori, T. Gotanda, Y. Nakano, M. Saito, K. Todori, M. Hosoya, *Jpn. J. Appl. Phys.* **2015**, *54*, 071602.
[35] R. Steim, T. Ameri, P. Schilinsky, C. Waldauf, G. Dennler, M. Scharber, C. J. Brabec, *Sol. Energy Mater. Sol. Cells* **2011**, *95*, 3256.
[36] B. P. Lechêne, M. Cowell, A. Pierre, J. W. Evans, P. K. Wright, A. C. Arias, *Nano Energy* **2016**, *26*, 631.
[37] F. Di Giacomo, V. Zardetto, G. Lucarelli, L. Cinà, A. Di Carlo, M. Creatore, T. Brown, *Nano Energy* **2016**, *30*, 460.
[38] H. K. Lee, Z. Li, J. R. Durrant, W. C. Tsoi, *Appl. Phys. Lett.* **2016**, *108*, 253301.
[39] Y. Aoki, *Org. Electron.* **2017**, *48*, 194.
[40] Y. J. You, C. E. Song, Q. V. Hoang, Y. Kang, J. S. Goo, D. H. Ko, J. J. Lee, W. S. Shin, J. W. Shim, *Adv. Funct. Mater.* **2019**, *29*, 1901171.
[41] P. C. Yang, I. M. Chan, C. H. Lin, Y. L. Chang, presented at *2011 37th IEEE Photovoltaic Specialists Conf.*, Seattle, WA, June **2011**.
[42] J. L. Lan, T. C. Wei, S. P. Feng, C. C. Wan, G. Cao, *J. Phys. Chem. C* **2012**, *116*, 25727.
[43] M. C. Tsai, C. L. Wang, C. W. Chang, C. W. Hsu, Y. H. Hsiao, C. L. Liu, C. C. Wang, S. Y. Lin, C. Y. Lin, *J. Mater. Chem. A* **2018**, *6*, 1995.
[44] K. Kawata, K. Tamaki, M. Kawaraya, *J. Photopolym. Sci. Technol.* **2015**, *28*, 415.
[45] Y. S. Tingare, N. S. Vinh, H. H. Chou, Y. C. Liu, Y. S. Long, T. C. Wu, T. C. Wei, C. Y. Yeh, *Adv. Energy Mater.* **2017**, *7*, 1700032.